AAPS PharmSciTech, Vol. 15, No. 5, October 2014 (© 2014)
DOI: 10.1208/s12249-014-0100-4

Research Article

Novel Dexamethasone-Loaded Nanomicelles for the Intermediate and Posterior Segment Uveitis

Ravi D. Vaishya,[1] Mitan Gokulgandhi,[1] Sulabh Patel,[1] Mukul Minocha,[2] and Ashim K. Mitra[1,3]

Received 6 September 2013; accepted 23 February 2014; published online 4 June 2014

Abstract. Development and characterization of dexamethasone (DEX)-encapsulated polymeric nanomicelles have been reported. A low molecular weight di-block copolymer was synthesized and characterized for its structure, molecular weights, critical micelle concentration (CMC), and cytotoxicity in ocular cells. In order to delineate the effects of drug–polymer interactions on drug solubilization in micelle core, a response surface methodology was generated with the help of SAS 9.02 (exploratory model). The method for preparing micelle was modified based on the results obtained from exploratory model. The formulation was optimized by response surface methodology (optimization model) to achieve DEX solubility of above 1 mg/mL. The optimized formulation was characterized for DEX solubility, nanomicelle size, polydispersity index, surface morphology, *in vitro* transport across conjunctival cell line, and *ex vivo* transport across excised rabbit sclera. Nanomicelles exhibited average sizes in range of 25–30 nm with unimodel size distribution and low polydispersity of 0.125. Nanomicelles increased DEX permeability by 2 times across conjunctival cell line and by 2.5 times across the excised rabbit sclera as compared to DEX suspension. A design of experiment (DOE) strategy was successfully applied to understand the effects of drug–polymer interaction on drug solubility. DOE was also employed to achieve optimal formulation with high DEX solubility. Nanomicellar formulation significantly enhanced DEX permeability across the excised rabbit sclera. Therefore, nanomicellar formulation may provide therapeutic levels in the back of the eye following topical administration.

KEY WORDS: design of experiment; dexamethasone; nanomicelles; ocular drug delivery; quality by design; response surface design; uveitis.

INTRODUCTION

Uveitis is an intraocular inflammatory disease responsible for 10–15% blindness in developed countries (1). It affects intermediate and/or posterior segments involving sections of choroid and retina, which often results in blindness. Steroids have been a mainstay treatment option for this inflammatory condition (2–5). Traditionally, steroids are administered by systemic routes. However, systemic administrations of steroid are not well tolerated by all patients (5,6). Topical drops of steroids are well tolerated, but drug levels achieved in intermediate and posterior ocular segments are often subtherapeutic (5,6). In the past decade, clinically recalcitrant uveitis has been treated by steroids administered as intravitreal (IVT) injections (4,7,8). IVT injections are associated with numerous side effects including retinal detachment, endophthalmitis, cataract, and elevated intraocular pressure (7,9).

Topical administration is the most patient-compliant route. Nonetheless, drug delivery to intermediate and posterior segment *via* topical drops is a significant challenge. Less than 5% of topically administered dose reaches ocular segments (such as retina and vitreous) owning to static and dynamic barriers (2,10). Typical instillation volume for topically administered formulation is usually less than 40–50 μL, to avoid drug loss *via* reflux tearing and nasolacrimal drainage. Low instillation volume entails steroidal agents to be solubilized at higher concentration in aqueous solution in order to achieve therapeutic drug level in intermediate and/or posterior segments. However, steroids are hydrophobic in nature with poor aqueous solubility and cannot be dissolved at higher concentrations in aqueous solution.

Nanocarriers such as liposomes and nanomicelles are capable of solubilizing highly hydrophobic drugs in aqueous medium (11–14). Micelles represent supramolecular

Electronic supplementary material The online version of this article (doi:10.1208/s12249-014-0100-4) contains supplementary material, which is available to authorized users.

[1] Division of Pharmaceutical Sciences, School of Pharmacy, University of Missouri-Kansas City, 2464 Charlotte Street, Kansas City, Missouri 64108-2718, USA.
[2] Center for Translational Medicine, School of Pharmacy, University of Maryland Baltimore, Baltimore, Maryland, USA.
[3] To whom correspondence should be addressed. (e-mail: mitraa@umkc.edu)

ABBREVIATIONS: DEX, Dexamethasone; DEXM, Dexamethasone-loaded nanomicelles; DOE, Design of experiments; IVT, Intravitreal; TBME, *tert*-Butyl methyl ether; mPEG, Methoxy polyethylene glycol; PCL, Polycaprolactone; RT, Root temperature; HCE, Human Conjunctival Epithelium; FBS, Fetal bovine serum; CMC, Critical micelle concentration; MTS, Nonradioactive cell proliferation assay; LDH, Lactate dehydrogenase.

arrangement of amphiphilic polymeric systems with typical size in range 10–100 nm. They have been investigated extensively to solubilize hydrophobic drugs. Polymeric micelles can be prepared with various di-block polymers consisting of hydrophobic and hydrophilic units. Transport of nanocarriers across the static and dynamic barriers depends on the particle size (15). Recently, Inokuchi *et al*. have illustrated that the liposome size of ~110 nm resulted in higher coumarin-6 accumulation in posterior segment following topical administration (16). A topical eye drop solution of steroids can be formulated by dissolving these compounds inside hydrophobic core of the polymeric micelles. We hypothesize that nanomicelles of mean size less than 50 nm may effectively overcome the static and dynamic barriers to provide therapeutic drug concentration in the intermediate and posterior uvea.

Recently, there is a growing interest in utilizing design of experiment (DOE) to optimize formulations. Experimental designs such as a three-level response surface methodology may explain the influence of individual factors and their interactions on response variables. In this manuscript, we have successfully employed DOE to understand the process parameters (dexamethasone (DEX)–polymer interaction in this case) on drug solubilization in micelles. Based on the information obtained from exploratory model, we modified the micelle preparation method to develop optimal formulation. The optimal formulation was characterized for micelle size, drug solubility, surface morphology, and *in vitro* drug release. Furthermore, *in vitro* transports across conjunctival cells and *ex vivo* transport across the excised rabbit sclera were also carried out for optimized formulation.

MATERIAL AND METHODS

Materials

Dexamethasone (purity ≥99%) was obtained from Enzo Life Sciences (Farmingdale, NY). ε-Caprolactone, stannous octoate, and methoxy poly(ethylene glycol) (mPEG; molecular weight (Mw) 2,000) were procured from Sigma Chemicals (St. Louis, MO, USA). Acetonitrile, methanol, D6-chloroform, D6-DMSO, anhydrous diethylether, and *tert*-butyl methyl ether (TBME) were also obtained from Sigma Chemicals (St. Louis, MO, USA) and used without further purification. Human conjunctival epithelial cell (HCE cell, Chang cell, CCL-20.2) was procured from the American Type Culture Collection (ATCC). Human corneal epithelial cell (SV40) was a generous gift from Dr. Araki-Sasaki (Kinki Central Hospital, Japan). Lactate dehydrogenase (LDH) and CellTiter 96® AQ_{ueous} Non-Radioactive Cell Proliferation (MTS) assay kits were purchased from Fisher Scientific Inc. and Promega Corp., respectively. Millipore™ Millex™ sterile syringe filters made of durapore hydrophilic polyvinylidene fluoride (PVDF) (pore size 0.22 μm) were obtained from Fisher Scientific.

Methods

Synthesis of di-Block Polymer

The di-block polymer was synthesized by ring opening polymerization by following published protocol with necessary modifications (17,18). Briefly, monomer ε-caprolatone (39.4 mmol), initiator mPEG (3 mmol), and catalyst stannous octoate (0.5% *w*/*w* of reactants) were added in a reaction vessel prefilled with nitrogen. Toluene (5 mL) was added to reactants, followed by heating at 100°C under vacuum until the total volume was reduced to initial volume. The temperature was then raised to 130°C. After 12 h, the reaction mixture was cooled down to room temperature (RT). The reaction mixture was dissolved in dichloromethane and precipitated in cold anhydrous ether. The final product was filtered and dried under vacuum. The polymer was characterized by ^{1}H-NMR (Varian 400 MHz), IR spectroscopy, and gel permeation chromatography for structure and molecular weight determinations.

Critical Micelle Concentration (CMC)

CMC was determined using pyrene as a hydrophobic fluorescent probe following a previously published method with modifications (19,20). Briefly, serial dilutions of polymer from 1,000 to 0.27 μg/mL were prepared in chloroform. Each dilution was added with 30 μg pyrene in chloroform. The chloroform solution, containing polymer and pyrene, was vortexed and dried under vacuum. DDW was added to the dried samples and vortexed for 1 min. Solutions were incubated at 37°C for 12 h then syringe-filtered (0.25 μm) to remove undissolved pyrene. Filtrates were measured for pyrene fluorescence. Samples were excited at 330 nm and emissions were measured at 372 nm (I_2) and 392 nm (I_1). A ratio of emission intensities (I_2/I_1) was plotted against polymer concentrations to calculate CMC. The polymer concentration where we observed a sharp increase in I_2/I_1 ratio was considered as CMC for the polymer.

Cell Culture

HCE cells were maintained in a cell culture flask containing Minimum Essential Medium (MEM) Earle's Balanced Salt Solution (BSS) medium supplemented with 10% fetal bovine serum (FBS), 100 U/L of penicillin, 100 mg/L of streptomycin, sodium bicarbonate (2.2 mg/mL), and 2 mM L-glutamine. Human corneal epithelial cells (SV40 cells) were cultured in DMEM/F-12 medium supplemented with 15% (*v*/*v*) heat-inactivated FBS, 22 mM $NaHCO_3$, 15 mM HEPES and 5 mg/L insulin, 10 μg/L human epidermal growth factor, 100 mg penicillin, and 100 mg streptomycin each. Both cell lines were incubated at 37°C, 5% CO_2, and 98% humidity.

In Vitro Cytotoxicity

Cytotoxicity studies were performed for newly synthesized polymer by MTS and LDH assays. Polymer concentrations of 25, 50, and 100 mg/mL were examined for cytotoxicity in both conjunctival (HCE cells) and corneal (SV40 cells) cell lines. The highest concentration of polymer in DOE was 53.8 mg/mL. The polymer concentrations were chosen such that it would cover the highest concentration of polymer in the final formulation obtained by DOE. We went up to 100 mg/mL concentration of polymer to make certain that there is no toxicity even at higher concentration.

MTS Assay. MTS assay was performed according to previously published protocol with minor modifications (21).

Polymer solutions were prepared in culture medium and sterilized by filtration with 0.2-μm syringe filters. In brief, HCE or SV40 cells at a density of 10^4 per well were cultured in a 96-well plate and incubated for 24 h. Polymer solutions were prepared in culture medium and sterilized by filtration with 0.2-μm syringe filters. Following incubation, medium was removed and cells were exposed to three different concentrations of polymer solution, *i.e.*, 25, 50, and 100 mg/mL (n=6). Cells without treatment were selected as positive control whereas cells treated with Triton-X 100 (0.1% *v*/*v*) as negative control. Following 48 h of incubation, culture medium from the 96-well plate was substituted by 100 μL of serum-free medium containing 20 μL of MTS solution. Cells were then incubated at 37°C and 5% CO_2 for 4 h. After incubation, absorbance of each well was measured at 450 nm. Cell viability (%) was calculated by Eq. 1.

$$\text{Cell viablity}(\%) = ((\text{Abs of sample} - \text{Abs of negative control}) / (\text{Abs of positive control} - \text{Abs of negative control})) \times 100 \quad (1)$$

LDH Assay. HCE or SV40 cells were seeded in 96-well plate at a density of 10^4 cells per well and incubated at 37°C, 5% CO_2, and 98% humidity for 24 h. Polymer solutions were prepared in culture medium and sterilized by filtration with 0.2-μm syringe filters. Following incubation period, cells were exposed to various concentrations of polymer (25, 50, and 100 mg/mL, n= 6) and incubated for 48 h. Cells without treatment were selected as negative control whereas cells treated with Triton-X 100 (0.1% *v*/*v*) as positive control. According to the protocol provided by the manufacturer, LDH release in cell supernatant was quantified by LDH assay kit (Takara Bio Inc., Japan). Samples were analyzed at an absorbance wavelength of 450 nm with 96-well plate reader. LDH (%) release was calculated by Eq. 2.

$$\text{LDH released}(\%) = ((\text{Abs of sample} - \text{Abs of negative control}) / (\text{Abs of positive control} - \text{Abs of negative control}) \times 100 \quad (2)$$

Exploratory Model (Experimental Design 1, ED 1)

In order to understand the factors and interactions influencing DEX solubilization in nanomicelles, a two-factor three-level response surface design (RSD) was employed. The factors under investigation were polymer amount ($X1$) and dexamethasone amount ($X2$) for their effects on DEX solubility (Y) in nanomicelles. The experimental design was generated with statistical design software SAS 9.02. The RSD-small composite Hartley method was utilized for the aforementioned independent variables and dependent variables (Table I). The primary reason for selecting this design is the least number of runs as compared to other designs. The design had nine runs in total, including three center points. DEX-loaded micelles were prepared by film hydration method (method 1).

Statistical Analysis. The influence of two factors (polymer ($X1$) and DEX ($X2$) amount) on one dependent variable was studied in an exploratory model. Hence, a statistical model with interactive and polynomial terms was used to evaluate their influence on the response variable (Y) (Eq. 3).

$$Y = b_0 + b_1X1 + b_2X2 + b_3X1X2 + b_4X1X1 + b_5X2X2 \quad (3)$$

where Y is a response variable (DEX solubility, mg/mL); $b0$ represents the intercept; $b1$, $b2$, $b3$, $b4$, and $b5$ represent the regression coefficients for factor and interactions. $X1$ (polymer amount in mg) and $X2$ (DEX amount in mg) are individual effects. $X1X1$ and $X2X2$ are polynomial terms of individual effects, which represent the polymer–polymer and drug–drug interactions, respectively. $X1X2$ is the interaction term representing drug–polymer interaction.

Results from this design were analyzed with one-way analysis of variance (ANOVA). F test was carried out at α=0.05 to determine the significance of regression relationship between the response variable (Y) and a set of independent variables. Significant factors and interactions were identified by t test at 95% significance level. R^2 and adjusted R^2 were also calculated for the regression model. The model was validated by checking model assumptions and lack of fit test. Statistical analysis was performed with SAS 9.02 and JMP 9.0.

Preparation of Nanomicelles (Method 1)

DEX-loaded nanomicelles, here on referred to as DEXM, were prepared by film hydration method. Calculated amount of polymer and DEX was accurately weighed out and dissolved in acetone/chloroform mixture (1:1). Organic solvents were evaporated under vacuum in a desiccator for 24 h to generate films. Films were then added with 1 mL of distilled deionized water (DDI) (65°C) and vortexed for 3 min. Nanomicellar solutions were syringe-filtered (0.22 μm) to separate undissolved DEX and subsequently analyzed for DEX content by reverse phase high-performance liquid chromatography (HPLC).

Preparation of Nanomicelles (Method 2)

Method 1 was modified based on the results obtained from exploratory model to obtained higher drug dissolution in nanomicelle core. The modified method is as follows. Briefly, drug and polymer films were obtained as described in method 1. The films were then heated at 65°C for 15 min to allow melting of the semicrystalline polymer. The melted films were added with 1 mL DDI water (37°C) and vortexed for ~45 s. The solutions were allowed to cool down to RT and filtered through 0.22-μm syringe filters. Clear micellar solutions were analyzed for DEX solubility by reverse phase HPLC.

Table I. Design Runs and Solubility of Dexamethasone for ED 1 (Micelle Preparation Method 1)

	Coded design		Uncoded design		Solubility
	Polymer	Dexamethasone	Polymer	Dexamethasone	
Run no.	*X*1	*X*2	*X*1	*X*2	*Y* (mg/mL)
1	−1	−1	10	1	0.26
2	1	1	50	5	0.37
3	−1.19	0	6.2	3	0.18
4	1.19	0	53.8	3	0.24
5	0	−1.19	30	0.6	0.20
6	0	1.19	30	5.4	0.30
7	0	0	30	3	0.27
8	0	0	30	3	0.27
9	0	0	30	3	0.33

Predictive Model (Experimental Design 2, ED 2)

The primary goal of ED 2 was to predict optimal DEX/polymer ratios providing DEX solubility of ≥1 mg/mL. Hence, ED 2 could also be referred to as the predictive model. We were also interested in delineating the effect of melting (micelle preparation method 2) on DEX solubility. RSD-small composite Hartley method described earlier was employed to achieve these goals (Table I). Based on experiments with method 1, we considered that DEX solubility of 1 mg/mL would be a significant increase. Hence, DEX solubility of 1 mg/mL was set as optimal/target value. Statistical treatment described in earlier section was applied to this design as well. In addition, a reduced model was generated by removing insignificant effects. The reduced model was utilized to predict the DEX/polymer ratio providing optimal DEX solubility and validated by checking model assumptions, lack of fit test, and check point analysis.

Micelle Size, Polydispersity, and Surface Morphology

Mean micelle size and polydispersity index (PDI) were determined with Zeta Sizer (Zetasizer Nano ZS, Malvern Instruments Ltd, Worcestershire, UK) at RT. A 500–750-μL solution was used without any dilution. Morphology of nanomicelles was examined by transmission electron microscopy (TEM) (Philips CM12 STEM). About 50 μL of micellar solution was placed on a carbon-coated copper grid. The excess of solution was removed by Kimwipe. Samples were negatively stained by phosphotungstic acid and completely dried before taking TEM images.

Powder X-ray Diffraction (XRD)

XRD analysis was performed for DEX, polymer, dried DEX–polymer film and freeze dried DEXM formulation. A Rigaku MiniFlex powder automated X-ray diffractometer (Rigaku, The Woodland, TX, USA) was utilized for the analysis at RT. Cu Kα radiation (λ=1.5418 Å) at 30 Kv and 15 mA was utilized. The diffraction angle covered from 2Θ 4.0° to 45.0°, and a step of 0.05° with 3 s/step was applied. The diffraction patterns were processed using Jade 8 (Materials Data, Inc., Livermore, CA).

In Vitro Release of DEX

The release mechanism for DEX from nanomicelles was determined by *in vitro* release study in simulated tear fluid (STF compositions: 2 g $NaHCO_3$, 6.7 g NaCl, 0.08 g $CaCl_2{\cdot}2H_2O$, and deionized water was added up to 1 L, Tween-80 (0.5% *w*/*w*)) (22) with a dialysis method (23–25). The optimal formulation obtained from the ED 2 was prepared and characterized for initial drug content. A five hundred-microliter micellar solution was added in a dialysis bag (MWCO 2,000 Da). The bag was tied at both ends and immersed in 10 mL of STF containing Tween-80 (0.5% *w*/*w*) at 37°C. The release medium was replaced with fresh STF at predetermined time points. The amount of DEX released was quantified by a reverse phase HPLC method. Release study was performed in triplicates. The results were plotted as mean±SD. The release data was fitted for zero-order, first-order, Higuchi, and Korsmeyer-Peppas model to determine the kinetics of DEX release.

In Vitro Transport Across Conjunctival Cells

Transwell diffusion chamber system was utilized for determining *in vitro* permeability of DEX from DEXM across conjunctival cells following a published protocol. Cells were seeded at a density of 25,000 per well in 12-well collagen-coated Transwell® permeable inserts (Costar®) and grown until confluency by changing medium every alternate day. Prior to a transport experiment, cell monolayers grown on the Transwell® inserts were rinsed with Dulbecco's phosphate-buffered saline (DPBS) (pH 7.4) and incubated at 37°C for 10 min twice for both apical (AP) and basolateral (BL) sides. Transport was initiated by adding 400 μL of DEX suspension or DEXM (in DPBS, pH 7.4) to the donor chamber (AP side) of cells. DPBS pH 7.4 was added in receiver chamber (BL side). Transport experiment was conducted for 3 h. Samples (100 μL) were collected from the receiver chamber at predetermined time intervals of 15, 30, 45, 60, 90, 120, 150, and 180 min, and fresh DPBS pH 7.4 was replaced to maintain sink conditions in the receiver chamber. The samples were analyzed by liquid chromatography-mass spectrometry (LC-MS/MS) analysis following a previously published method from our laboratory

(26). Permeability (P_{app}) of DEX was calculated using Eq. 4.

$$P_{app} = M/A \times C_d \quad (4)$$

where M represents the slope obtained from the plot of cumulative amount of drug permeated *vs.* time, A denotes the surface area of membrane exposed to drug, and C_d is the drug concentration in donor chamber at $t=0$.

Transport study was conducted in quadruplicate for all test and control sets. A statistical significance between the permeability of DEX suspension and DEXM at $p<0.05$ was considered to be significant.

Ex Vivo Transport Across the Sclera (23)

Tissue Preparation. Adult New Zealand male rabbits weighing between 2 and 2.5 kg were obtained from Harlan laboratory. All animal handling procedures were approved by the Institutional Animal Care and Use Committee (IACUC) of the University of Missouri-Kansas City (UMKC, Kansas City, MO, USA). Rabbits were anesthetized with I.M. administration of ketamine HCl (35 mg/kg) and xylazine (5 mg/kg). The animals under deep anesthesia were euthanized by an overdose of sodium pentobarbital (100 mg/kg) administered through marginal ear vein. Eyes were removed carefully, and the posterior segment was separated by cutting along the limbus. Retina and choroid were separated from the sclera, and the sclera was placed in a petri dish containing Dulbecco's phosphate-buffered saline (pH 7.4).

In order to carry out permeability studies, the excised tissue was mounted on a Franz-type vertical diffusion cell (PermeGear Inc., Hellertown, PA, USA) with episcleral side facing the donor chamber. The receptor chamber was filled with isotonic phosphate-buffered saline (IPBS; pH 7.4). Dexamethasone suspension or DEXM formulation was added to the donor chamber to begin transport study. At a regular time interval, 200 μL of sample was withdrawn from the receptor chamber and replaced with an equal volume of fresh IPBS buffer. Experiments were carried under sink conditions for 3 h at 37°C in quadruplet. The samples were analyzed by LC-MS/MS following a method published previously from our laboratory (26). Permeability (P_{app}) was calculated according to Eq. 4.

HPLC Method

Reverse phase HPLC method described earlier was used with necessary modifications (27). Shimadzu LC pump (Waters, Milford, MA, USA) equipped with a UV detector (SPD-20AV, Shimadzu) was employed for the HPLC analysis. The mobile phase consisted of 65% tetrabutylammonium hydrogen sulfate (TBAHS) buffer and 35% acetonitrile (ACN) on a reverse phase C18 column (Phenomenex C18 Kinetex column 100×4.6 mm, 5 μm) as a stationary phase. Mobile phase flow rate was set at 0.4 mL/min. UV detector was set at 254 nm for quantifying DEX.

Analysis of DEX in Buffer Samples by LC-MS/MS

The LC-MS/MS method described earlier from our lab (26) was utilized with a few modifications for quantitating DEX in buffer samples from *ex vivo* transport studies. Ninety-microliter aliquots of buffer samples were spiked with 20 ng of prednisolone (IS) and vortexed for 15 s. The analytes were then extracted with 900 μL of ice-cold TBME and vortexed for 3.5 min. Samples were centrifuged at 10,000 rpm for 7 min to separate the aqueous and organic layers. Seven hundred and fifty microliters of the organic layer was collected and dried in vacuum. Dried sample was reconstituted in 100 μL of mobile phase (ACN/water::40:60, 0.1% formic acid). Ten microliters of reconstituted sample was injected onto the LC-MS/MS for analysis. LC/MS-MS QTrap® API-3200 mass spectrometer, equipped with Shimadzu quaternary pump, vacuum degasser, and autosampler (Shimadzu Scientific Instruments, Columbia, MD, USA), was employed to analyze samples from *ex vivo* studies.

HPLC separation was performed on an XTerra® MS C18 column 50 mm×4.6 mm, 5.0 μm (Waters, Milford, MA, USA). The mobile phase consisted of 40% ACN and 60% water with 0.1% formic acid, pumped at a flow rate of 0.25 mL/min. Multiple reaction monitoring (MRM) mode was utilized to detect the compounds of interest. The mass spectrometer was operated in the positive ion mode for detection. The precursors to product ions (Q1→Q3) for DEX and IS during quantitative optimization were (m/z) 393.20→355.30 and 361.30→147.20, respectively. The operational parameters for the tandem mass spectrum for each analyte were obtained after running them in quantitative optimization mode. The turbo ion spray setting and collision gas pressure were optimized (IS voltage, ±5,500 V; temperature, 350°C; nebulizer gas, 40 psi; curtain gas, 30 psi). The lower limit of mL for DEX/mL for DEX.

RESULTS AND DISCUSSION

Synthesis and Characterization of Polymer

Di-block polymer was synthesized by anionic ring opening polymerization using stannous octoate as the catalyst and mPEG as the initiator. Polymer was purified by cold ether precipitation and dried under vacuum. Structure of the polymer was confirmed by ^{1}H-NMR (Fig. 1a) and Fourier transform infrared spectroscopy (FTIR) spectroscopies. Proton NMR showed all the characteristic peaks for the polycaprolactone and mPEG residues. FTIR spectroscopy of polymer showed the presence of terminal alcohol at 3,441.09 cm^{-1} and carbonyl group at 1,723.95 cm^{-1} (Supplementary info Figure 1). Weight and number average molecular weights (Mw and Mn) and PDI were determined by gel permeation chromatography. Mw, Mn, and PDI were determined to be 4,586 Da, 3,155 Da, and 1.45, respectively. CMC was obtained by pyrene method in aqueous polymer solution (Supplementary info Figure 2). CMC for the polymer was 4.5 μg/mL, indicating good stability against dilutions.

XRD analysis for the polymer showed presence of characteristic peaks for polycaprolactone (PCL) and mPEG suggesting semicrystalline nature of the polymer (Fig. 2b).

Cytotoxicity studies of the new polymer were conducted on conjunctival and corneal cells, by MTS and LDH assays, prior to the development of formulation. Percent cell viability was calculated based on amount of formazione released for both HCE and SV40 cells (MTS assay) (Supplementary information Figure 3). Positive control (medium) and test groups were compared by ANOVA. No significant difference in %cell viability was observed at all polymer concentrations (ANOVA $p>0.05$). In addition, cytotoxicity study was also performed by LDH assay to confirm the results obtained from the MTS assay. Polymers interact with cells *via* cell membrane, and therefore, estimating the amount of LDH released in culture medium could be a preferred way to estimate the cell wall damage and thus cytotoxicity of polymers. LDH release for cells treated with polymer was compared to negative control (blank, medium). Based on ANOVA analysis, no significant difference in %LDH release was observed between blank and treatment groups, in both HCE and SV40 cells (Supplementary information Figure 4).

Formulation Optimization

Exploratory Model (Experimental Design 1)

Preliminary experiments to prepare DEXM with film hydration method did not result in appreciable increase in solubility. Hence, a response surface methodology (small composite Hartley design) was employed to understand the influence of drug–polymer interactions on drug solubility in micelle core and identify the factors/interactions responsible for poor DEX loading in nanomicelles. The design runs (coded and uncoded runs) and corresponding DEX solubilities are presented in Table I. Solubility of DEX ranged from 0.18 to 0.37 mg/mL. Among all the runs, the highest solubility of DEX was observed for run no. 2 (0.37 mg/mL), where both drug and polymer were at their highest levels (+1). Statistical treatment explained earlier was applied to analyze the data. Second-order least square equation for the master model is given by Eq. 5.

$$Y = 0.28 + 0.0217 \times X1 + 0.0382 \times X2 + 0.1052 \times X1X2 - 0.0494 \times X1X1 - 0.02083 \times X2X2 \quad (5)$$

Master Model. Table II summarizes ANOVA, lack of fit, and correlation coefficient for the master model. The master model was found to be significant ($p=0.0155$), indicating that solubility of DEX (Y) was considerably dependent on the set of X variables. The correlation coefficient (R^2) for the regression model was 0.9720. It means that the model explains 97.2% of variation in DEX solubility. Lack of fit p value of 0.5953 also suggested that the master model was significant and could predict DEX solubility. The model was also validated based on the plot of actual *vs.* predicted solubility (Supplementary information). A linear relationship was observed between actual DEX solubilities and solubilities predicted by the model with R^2 of 0.97. Also percent standard error of residual was found to be less than 10% for all the runs (Supplementary information), suggesting the model was significant. Reduced model was not generated since the aim of the exploratory model was to delineate the influence of the set of X variables on DEX solubility.

Estimated coefficients for each term (factors and interactions) with associated p values are presented in Supplementary information Table 1. The estimated coefficients with $p<0.05$ were considered to be significant. Significant terms from the model were the amount of DEX ($X2$, $p=0.0156$), DEX–polymer interaction (X1X2, $p=0.0069$), and polymer–polymer interaction ($X1X1$, $p=0.0157$) as indicated by Pareto chart (Fig. 3). $X1X1$ had negative influence, while $X1X2$ and $X2$ had positive effect on DEX solubility. $X2X2$ also had negative effect on DEX solubility but the interaction was not significant ($p=0.1236$).

The response surface curve provides a diagrammatical representation of DEX solubility as a function of polymer and DEX amounts (Fig. 4). The response surface was found to be nonplanar. Interestingly, increasing the polymer amount had variable effects on DEX solubility depending on the amount of DEX. For example, at a high level of DEX (+1 or 5 mg), raising the polymer amount had positive influence on solubility of DEX, as anticipated. The increase in DEX solubility could be attributed to enhanced DEX–polymer interaction ($X1X2$), which was the most significant term according to master model ($p=0.0069$). Nonetheless, solubility increase was not linear; such nonlinearity could be attributed to $X1X1$ interaction in the dried film which may lower DEX solubility. On the contrary, increasing the polymer amount at low DEX level (−1 or 1 mg) resulted in a decrease in solubility. Moreover, the decline in solubility was steeper and nonlinear which may be explained by $X1X1$ interaction. At low level of DEX, $X1X1$ would be the dominant interaction compared to $X1X2$ which may explain the steeper decline in DEX solubility with an increase in X1.

To characterize the physical form of DEX and polymer, the dried polymer–DEX film was studied by XRD. Polymer/DEX film was prepared at a ratio X1:$X2$::30:5. XRD showed the presence of characteristic peaks of PCL ($2\theta=21.9$) and mPEG ($2\theta=19.2$ and 23.8) in the dried film (Fig. 4), suggesting that the $X1X1$ interaction represents crystallization of the polymer upon evaporation of organic solvent. Small peaks corresponding to DEX were also present ($2\theta=14$, 15.6, and 17) in the dried film, indicative of slight crystallization and $X2X2$ interaction. From the exploratory model, it can be concluded that solubility of DEX in micellar core is governed by polymer–DEX interaction ($X1X2$). We can also infer that polymer–polymer interaction ($X1X1$) occurs during solvent evaporation leading to significantly lower DEX entrapment. In order to improve DEX solubility, we need to overcome $X1X1$ interactions. In this case, $X1X1$ interaction

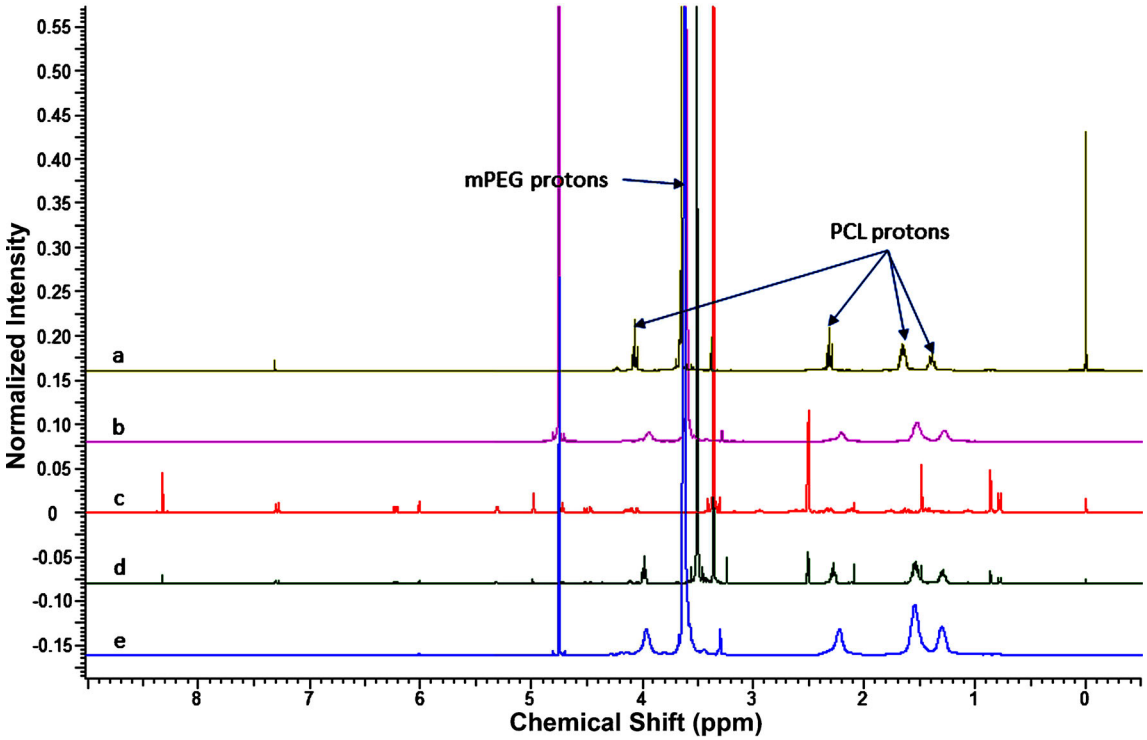

Fig. 1. ^{1}H-NMR spectroscopies for (*a*) PCL–mPEG polymer in $CDCl_3$, (*b*) blank PCL–mPEG micelles in D_2O, (*c*) dexamethasone in d_6-DMSO, (*d*) PCL–mPEG (50 mg) and dexamethasone (1 mg) in d_6-DMSO, and (*e*) 0.1% DEXM in D_2O

represents the crystallization of polymer. We hypothesize that heating the dried polymer–DEX film above the melting point of polymer (t_m=60–62°C) may overcome *X*1*X*1 interaction (nanomicelle preparation method 2). Lowering *X*1*X*1 interaction may allow free polymer to interact with DEX thus maximizing DEX entrapment in micelle core.

Optimization Model (Experimental Design 2)

Based on our hypothesis, in order to overcome *X*1*X*1 interaction, we modified nanomicelle preparation method 1. A response surface design as explained earlier for exploratory model was generated for independent variables polymer amount (X1) and DEX amount (*X*2) and response variable

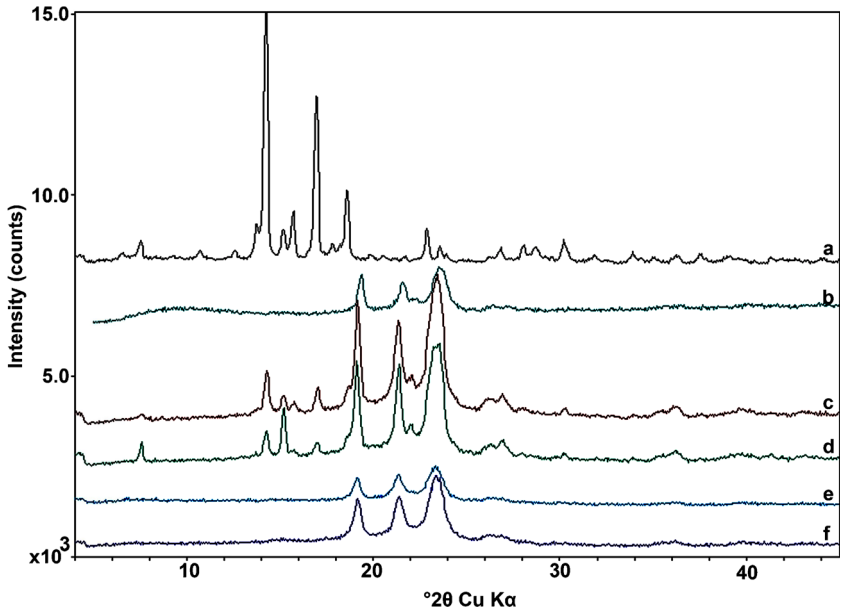

Fig. 2. X-ray diffraction pattern for (*a*) dexamethasone, (*b*) PCL–mPEG polymer, (*c*) polymer/DEX film before heating (polymer/DEX::30:5), (*d*) polymer/DEX film after heating (polymer/DEX::30:5), (*e*) freeze-dried blank micelles, and (*f*) freeze-dried DEXM (0.1% *w*/*v* DEX)

Table II. Summary Statistics for Master Model (ED 1)

Summary of fit					
*R*Square	0.9720				
RSquare Adj	0.9253				
Analysis of variance					
Source	*DF*	Sum of squares	Mean square	*F* ratio	Prob>*F*
Model	5	0.0249	0.0050	20.8257	0.0155
Error	3	0.0007	0.0002		
C. total	8	0.0256			
Lack of fit					
Source	*DF*	Sum of squares	Mean square	*F* ratio	Prob>*F*
Lack of fit	1	0.0001	0.0001	0.3917	0.5953
Pure error	2	0.0006	0.0003		
Total error	3	0.0007			

DF degrees of freedom

DEX solubility (Y). DEXM were prepared by modified film hydration method (method 2). Table III summarizes design runs (uncoded design), DEX solubility for each run, micelle size, and PDI. Highest solubility of 1.36 mg/mL was obtained for design run no. 4.

Master Model. Quadratic equation for the master model is given by Eq. 6,

$$Y = 0.7337 + 0.4374 \times X1 + 0.0455 \times X2 + 0.0132 \times X1X2 + 0.0338 \times X1X1 - 0.0638 \times X2X2 \quad (6)$$

Statistical parameters for the master model including parameter estimates, ANOVA for the master model, and lack of fit analysis are summarized in Table IV. The master model was found to be significant, based on model p value ($p=0.0128$), lack of fit p value ($p=0.0901$), and adjusted R^2 of 0.9345. The parameter estimates for master model are shown in Supplementary info Table 2. According to the Pareto chart, only statistically significant factor was polymer amount (X1, $p=0.0026$), unlike method 1 where polymer amount did not have any significant effect on DEX solubility (Fig. 5a). This result may be attributed to melting of polymer in the film that allowed polymer to overcome $X1X1$ interaction, as we hypothesized. No influence of $X1X1$ interaction on drug solubility ($p=0.5858$) was observed with modified film hydration method. XRD analysis of dried DEX–polymer film was conducted after heating the films to delineate the effect of heating on physical form of polymer. DEX–polymer film was prepared at 30:5::X1:$X2$ ratio. The peaks for mPEG-PCL were present despite heating the film at 65°C (Fig. 5). These results could be explained by the fact that XRD patterns were recorded at RT. Gradual cooling of DEX–polymer film to RT could result in the recrystallization of polymer. It also worth noting that heating the film did not have any effect on the physical form of DEX, as predicted (Fig. 5a).

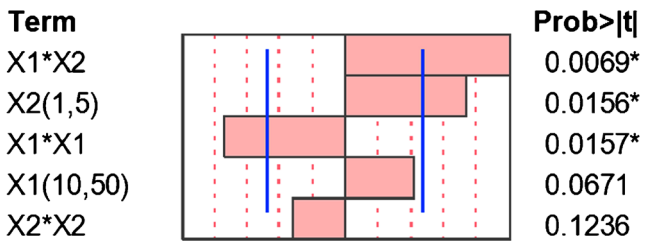

Fig. 3. Pareto chart for master model (ED 1). *Asterisk* next to p value represents significant term

Reduced Model. A reduced or predictive model was generated by removing the nonsignificant terms with $p>0.05$ from the master model. Hence, terms $X1X2$ and $X1X1$ were removed. XRD analysis indicated crystallization of DEX in polymer–DEX film (after heating) representing $X2X2$ interaction (Fig. 5). In addition, removing the $X2X2$ interaction did

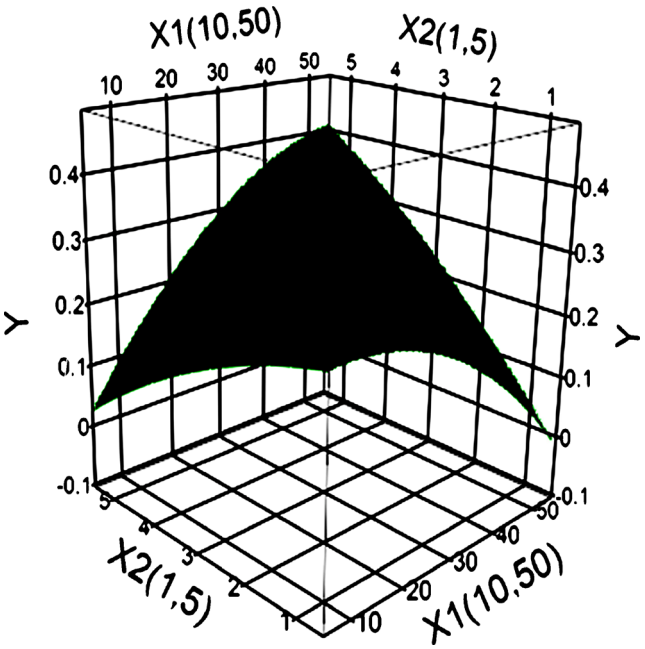

Fig. 4. Response surface for master model (ED 1). DEX solubility (Y) is plotted as a function of polymer ($X1$) and DEX ($X2$) amounts between −1 and 1

Table III. Summary of Uncoded Design and Corresponding Solubility, Micelle Size, and PDI for ED 2 (Micelle Preparation Method 2)

Run	Polymer *X*1 (mg)	Dexamethasone *X*2 (mg)	Solubility *Y* (mg/mL)	Size (nm)	PDI
1	10	1	0.30	26.44	0.094
2	50	5	1.13	27.32	0.125
3	6.2	3	0.21	27.99	0.070
4	53.8	3	1.36	28.01	0.135
5	30	0.6	0.53	28.38	0.100
6	30	5. 4	0.75	28.98	0.225
7	30	3	0.68	27.79	0.076
8	30	3	0.75	27.99	0.122
9	30	3	0.77	27.17	0.106

DF degrees of freedom, *PDI* polydispersity index

not improve the model p value, lack of fit p value, or adjusted R^2 (data not shown). Hence, the term $X2X2$ was not removed from the master model. Summary statistic for the reduced model is presented in Table V. The predictive model was compared with the master model for p values of the model, p value of lack of fit, and adjusted R^2. The reduced model had a p value of 0.0003, lack fit p value of 0.2056, and adjusted R^2 of 0.9524, indicating that the reduced model was superior in predicting DEX solubility (Y). The parameter estimates for the reduced model are shown in Supplementary info Table 3. Pareto chart for the reduced model is depicted in Fig. 5b. Again, the only significant term influencing DEX solubility was $X1$ ($p=$ 0.0001). Interactions between DEX molecules ($X2X2$) were not significant ($p=0.1673$) as per model and, as expected, had negative effect on DEX solubility with method 2. Similar observation was noted for method 1 (exploratory model) suggesting that the melting has no influence on DEX crystallization. The prediction expression for reduced model is presented by Eq. 7,

$$Y = 0.756 + 0.437 \times X1 + 0.046 \times X2 - 0.066 \times X2X2 \qquad (7)$$

Response surface showing the change in solubility of DEX as a function of DEX and polymer amounts is illustrated in Fig. 6. Unlike the exploratory model, we were able to overcome the negative effect of $X1X1$ on DEX solubility with the modified method. Hence, the solubility of DEX increased linearly with increasing polymer amount at all the DEX levels. Nonetheless, solubility increase was not linear with increasing DEX amount due to $X2X2$ interaction. In addition, despite the ratio for the DEX/polymer is the same in runs 1, 2, and 7, the amounts of polymer and DEX are different (Table V). These different amounts resulted in variable solubility of DEX depending on the strength of DEX × DEX, polymer × DEX, and polymer × polymer interactions in the film upon drying. Hence, we see different solubilities for DEX at same DEX/polymer ratios. Furthermore, upon overcoming X1 × X1 interaction in optimized method 2, a significant enhancement in the solubility of DEX was observed (Tables V and VI) for the same amount of DEX and polymers. For example, the solubility of DEX was 0.37 and 1.13 mg/mL at 50 mg polymer and 5 mg DEX with methods 1 and 2, respectively (run no. 2 in Tables V and VI).

The prediction profile was generated to determine the optimal point with the highest desirability (Supplementary info Figure 5). The check point analysis was carried out to validate the reduced model at $X1$:$X2$::20:2 ratio. Ratio $X1$:$X2$::20:2 was selected for check point analysis as it was not a part of design runs suggested by the statistical software (SAS 9.02). No statistically significant difference was observed between experimental and predicted DEX solubility ($p>0.05$) (Table VI).

The model was also validated by plotting predicted *vs.* actual solubility (Supplementary info Figure 6). The relationship was found to be linear with R^2 of 0.97 indicating predicted solubility by model is close to experimental one. The residuals

Table IV. Summary Statistics of Master Model [ED 2]

Summary of fit					
RSquare	0.9754				
RSquare Adj	0.9345				
Analysis of variance					
Source	*DF*	Sum of squares	Mean square	*F* ratio	Prob>*F*
Model	5	1.0303	0.2061	23.8266	0.0128
Error	3	0.0259	0.0086		
C. total	8	1.0562			
Lack of fit					
Source	*DF*	Sum of squares	Mean square	*F* ratio	Prob>*F*
Lack of fit	1	0.0215	0.0215	9.6167	0.0901
Pure error	2	0.0045	0.0022		
Total error	3	0.0259			

DF degrees of freedom

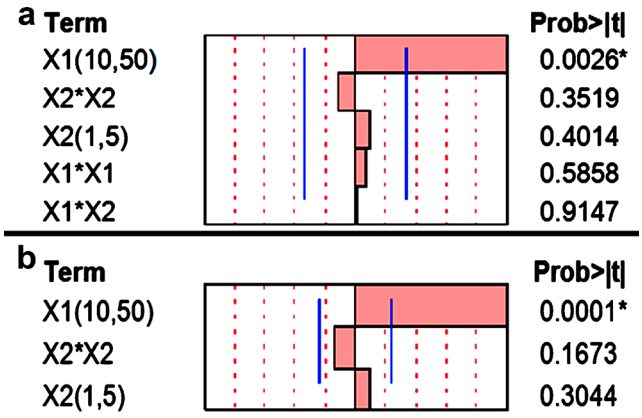

Fig. 5. **a** Pareto chart for master model (ED 2). **b** Pareto chart for reduced model (ED 2). *Asterisk* next to *p* value represents significant term

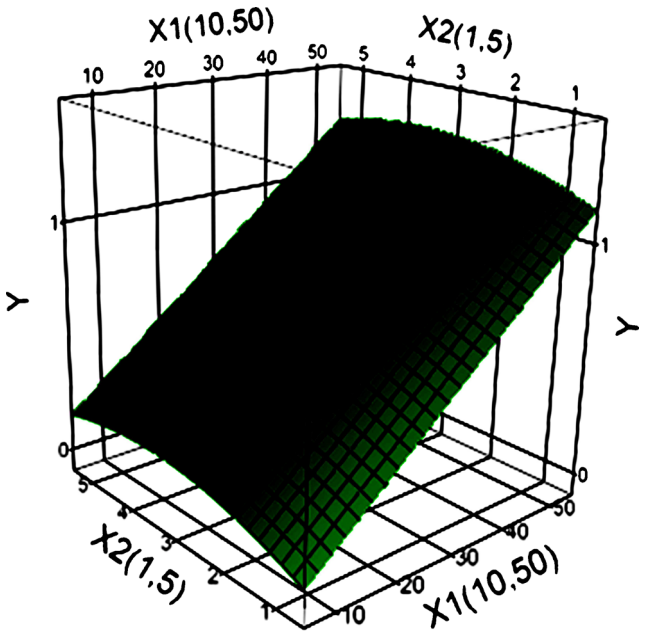

Fig. 6. Response surface of predictive model for ED 2. DEX solubility (*Y*) is plotted as a function of polymer (*X*1) and DEX (*X*2) amounts between −1 and 1

and percent standard errors for each run of design are presented in Supplementary info Table 4. Standard error (%) was less than 10% for all the runs. Based on the check point analysis, percent standard error of residual, and experimental *vs.* predicted solubility, it was concluded that the reduced model can accurately predict DEX solubility. Using prediction profile for reduced model, optimal *X*1:*X*2 ratio to obtain DEX solubility ≥1 mg/mL was obtained.

Characterization of Formulation

Micelle Size and Morphology

Nanomicelle size and distribution were determined by dynamic light scattering method for all the runs in ED 2. The results are presented in Table VI. The size ranged from 26 to 28 nm with unimodel distribution irrespective of DEX solubility. The PDI for all the runs were below 0.23 indicating narrow size distribution. Size distribution showing mean size and PDI for design run no. 2 is illustrated in Fig. 7a. The average size was 27.32 nm with PDI of 0.125. It is expected that micelle size would increase with an increase in DEX solubility from 0.21 to 1.36 mg/mL. However, it is worth noting that even with this increase in solubility, drug loading did not vary appreciably (data not shown). Hence, we did not observe an appreciable increase in nanomicelle size or polydispersity with an increase in solubility. The morphology of optimal nanomicelle was studied by TEM (Fig. 7b). TEM micrograph of nanomicelles indicated that the nanomicelles were spherical in shape.

^{1}H-NMR Spectroscopy of Blank Micelles and DEXM

Processes of micelle formation and DEX encapsulation in micelle core were studied with proton NMR spectroscopy. ^{1}H-NMR for blank PCL-mPEG micelles was recorded in D_2O and compared with NMR spectra in $CHCl_3$. Weak ^{1}H-NMR signal from PCL protons in D_2O clearly indicated nanomicelle formation (Fig. 7). During micelle formation, PCL block assembles to form the hydrophobic core and mPEG segment forms hydrophilic corona. Since the core of micelle lacks accessibility to solvent, movement of PCL segment in the core is limited and hence the proton NMR signal is very weak compared

Table V. Summary Statistics of Reduced Model for ED 2

Summary of fit					
RSquare	0.9703				
RSquare Adj	0.9524				
Analysis of variance					
Source	*DF*	Sum of squares	Mean square	*F* ratio	Prob>*F*
Model	3	1.0248	0.3416	54.3875	0.0003
Error	5	0.0314	0.0063		
C. total	8	1.0562			
Lack of fit					
Source	*DF*	Sum of squares	Mean square	*F* ratio	Prob>*F*
Lack of fit	3	0.0269	0.0090	4.0205	0.2056
Pure error	2	0.0045	0.0022		
Total error	5	0.0314			

DF degrees of freedom

Table VI. Check Point Analysis for Reduced Model (ED 2)

*X*1:*X*2 ratio	Predicted solubility (mg/mL)	Experimental solubility (mg/mL)	Two-tailed *p* value	% Standard error
20:2	0.499±0.093	0.588±0.038	0.3666	5.8
50:3.5	1.201±0.127	1.146±0.166	0.6722	1.21

to signal in $CDCl_3$. In contrast, the corona-forming mPEG segment is free to move in D_2O showing good ^{1}H-NMR signal intensity.

^{1}H-NMR spectroscopy was also used to ascertain the presence of DEX in nanomicelle core. ^{1}H-NMR spectra for the physical mixture of DEX and polymer in d_6-DMSO, DEXM in D_2O, and DEX in d_6-DMSO were recorded (Fig. 7). The ^{1}H-NMR spectra for the combination of DEX and polymer in d_6-DMSO showed all the characteristic peaks corresponding to DEX, PCL, and mPEG (Fig. 7). ^{1}H-NMR for DEXM in D_2O also showed the presence of characteristic peak for mPEG segment at 3.4–3.6 ppm and those for PCL were absent, indicating micellization. Characteristic peaks for DEX were absent due to restricted mobility inside micelle core, implying that drug was molecularly dispersed in micelle core (Fig. 7).

Powder XRD Analysis of Blank Micelles and DEXM

Blank micelles and DEXM were also studied by XRD to seek further insight into physical state of polymer and DEX in nanomicelles. The results are presented in Fig. 7. XRD pattern for freeze-dried DEXM was devoid of DEX peaks indicating that the drug was molecularly dispersed in nanomicelle. Both blank micelles and DEXM showed characteristic peaks for PCL at 2θ 19° and 23°. PCL, due to its semicrystalline nature, does not self-assemble in water to form micelles at RT. However, temperatures close to melting point provide PCL with necessary chain mobility to self-assemble into micelles. Once the micelles are formed and system reaches RT, PCL segments in core reestablish the polymer–polymer interactions regaining its semicrystalline state in nanomicelle core. We expect that the semicrystal nature of nanomicelle core would provide rigid core to the nanomicelles. Such rigid micelle core may provide resistance against sheer stress while transporting nanomicelles across the scleral pores. Rigidity has been shown to be beneficial for liposomal formulation during transport across the sclera (16).

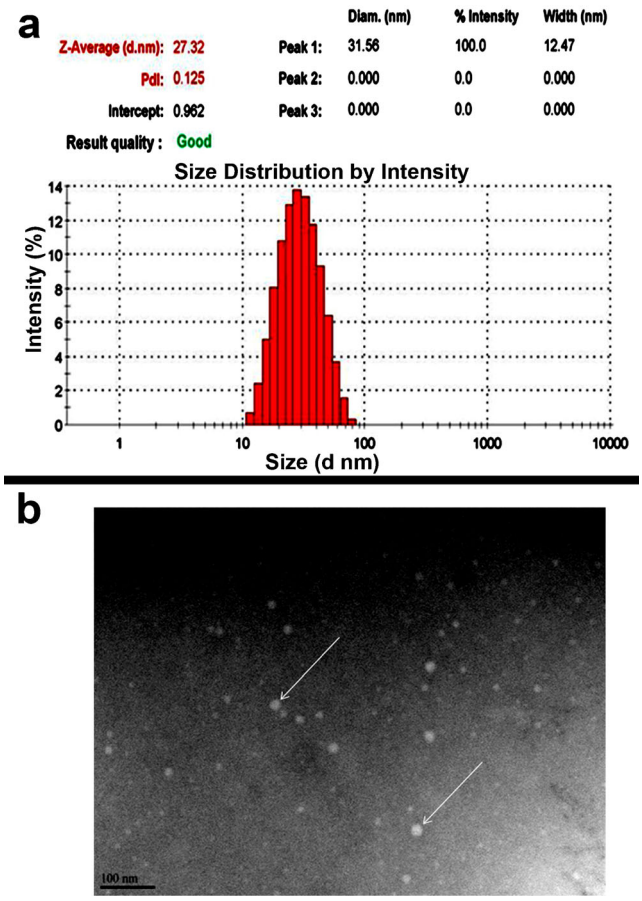

Fig. 7. **a** Transmission electron micrograph for DEXM. Nanomicelles appear as a white spot on dark background as indicated by *arrows*. **b** Micelles size distribution for DEXM for design run no. 2 of ED 2

Release Kinetics of DEX

The release study was performed in simulated tear fluid at 37°C, under sink condition, to identify the mechanism of

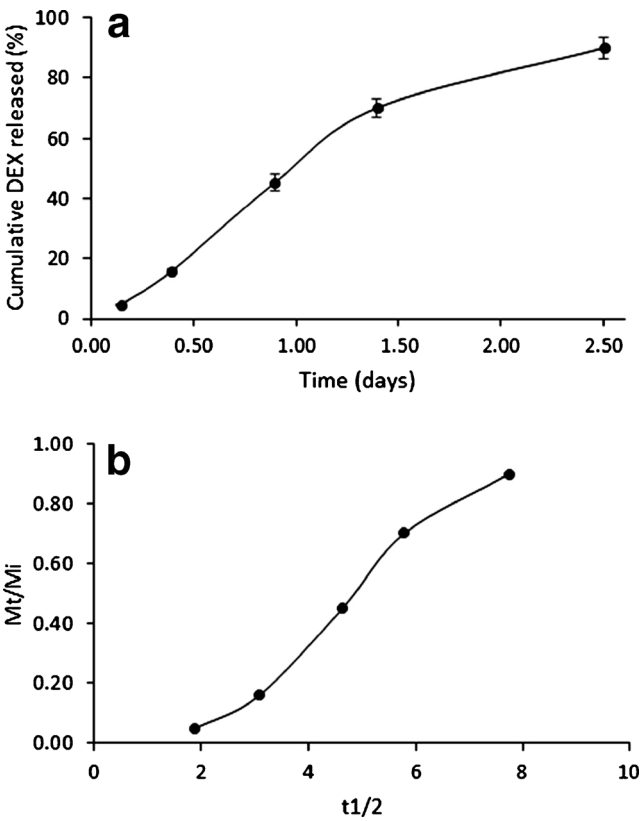

Fig. 8. **a** Release profile of dexamethasone from nanomicelles under sink conditions at 37°C (mean±SD, n=4). **b** Fraction of DEX released at time t (Mt/Mi) vs. $t^{1/2}$ profile showing sigmoidal shape suggesting case II transport as the drug release mechanism

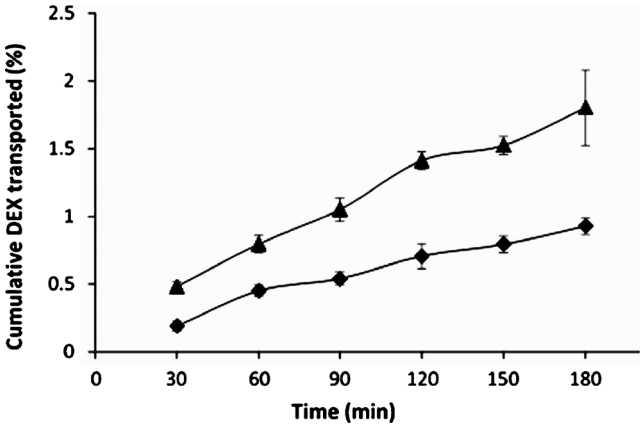

Fig. 9. Cumulative percent dexamethasone transport across conjunctival cells *vs.* time profile for dexamethasone suspension (*black diamond*) and DEXM (*black triangle*). (Data are presented as mean±SD, $n=3$)

DEX release from nanomicelles. Cumulative %DEX released *vs.* time profile is illustrated in Fig. 8a. DEX release from the nanomicellar system lasted for 2.5 days. About 50% DEX was released by 24 h from nanomicelles. Previously, it has been shown that mPEG-PCL could sustain the release of hydrophobic agent such as honokiol (log p 5.21, polar surface area 40.46 (28)) for up to 2 weeks (29). However, DEX is relatively polar molecule with log p of 1.68 and large polar surface area of 94.83 (30). This may be responsible for poor interaction with hydrophobic PCL chains resulting in relatively faster release pattern.

Release data was fitted to zero-order, first-order, Higuchi, and Korsmeyer-Peppas model to determine the kinetics of DEX release. The best fit was found with the Korsmeyer-Peppas model with an R^2 of 0.9998 compared to other models. The n value was calculated using the data points where less than 60% DEX was released. The n value was found to be 1.24 suggesting super case II transport as release mechanism. In super case II transport, drug release is controlled mainly by the polymer chain relaxation (31). The polymer chain relaxation may result in the loss of DEX–polymer interaction which encapsulates DEX in micelle core. In addition, due to the semicrystalline nature of PCL chains, upon release of DEX from micelles, the polymer chain will have more freedom to align and form rigid crystalline core. Formation of rigid core upon release will also hinder the repartition of DEX back in nanomicelle core. Furthermore, the volume of release medium was 10 mL with Tween-80 (0.5% *w*/*w*) which would aid solubilization-released DEX. To further confirm super case II release mechanism, the fraction of drug release (Mt/Mi) as a function of square root of time ($t^{1/2}$) was plotted. The graph had a sigmoidal shape suggesting the mechanism was indeed super case II transport (Fig. 8b).

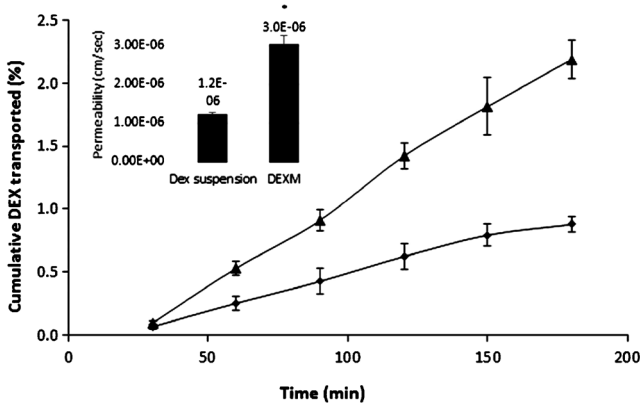

Fig. 10. Cumulative percent dexamethasone transported across the excised rabbit sclera *vs.* time profile for dexamethasone suspension (*black diamond*) and DEXM (*black triangle*). The *inset* shows apparent permeabilities for DEX with DEXM and DEX suspension (*$p<0.05$) (Data are presented as mean±SD, $n=3$)

In Vitro Transport Across Conjunctival Cells

We intend to use the nanomicelles for drug delivery to interior and posterior segment *via* topical administration. Hence, we also examined DEX transport across conjunctival cells (*in vitro*) and excised rabbit sclera (*ex vivo*). Figure 9 illustrates cumulative percent DEX transported across conjunctival cells from nanomicelles and suspension. The permeability of DEX with nanomicelles was 1.3E–06 cm/s, which was ~2 times higher relative to DEX suspension (0.69E–06 cm/s).

Transscleral Permeability of DEX

The sclera acts as a static barrier for transport of drug/nanocarriers towards back of the eye following topical administration. Hence, transport of DEX across the excised rabbit sclera was carried out for the nanomicelles and compared with DEX suspension (0.1% *w*/*v*). Cumulative percent DEX *vs.* time profile for DEXM and DEX suspension is illustrated in Fig. 10. The inset represents average permeabilities. A statistically significant increase in DEX permeability was observed with DEXM (P_{app}=3.0E–06 cm/s) relative to DEX suspension (P_{app}=1.19E–06 cm/s; $p<0.05$). A 2.5-fold increase in permeability with nanomicelles indicates a possible influence of nanomicelle size on DEX transport across the sclera. The increase in permeability with nanomicelles could be attributed to transport through the aqueous scleral pores (32). We hypothesized that nanomicelles could improve the bioavailability of DEX in the uvea following the topical administration. Also, the conjunctival–scleral route could be of more importance compared to the corneal route in order to achieve higher intraocular levels. Conjunctival–scleral route could be favored due to high surface area and absence of tight junctions like in the cornea. Nanomicelles exhibited significantly high permeabilities for transport across the conjunctival cell line and sclera. Based on these preliminary experiments, we could suggest that there is a high possibility of achieving elevated DEX levels in the intraocular tissues (uveal track) *via* conjunctival–scleral route. In addition, the release of DEX from nanomicelles was relatively slower and lasted for more than 2 days. Thus, the frequency of topical administrations could also be reduced increasing patient compliance. However, further *in vivo* experiments are necessary to confirm this hypothesis.

CONCLUSIONS

Small molecular weight di-block copolymer was successfully synthesized and characterized for its molecular weight, PDI, cytotoxicity on conjunctival and corneal cells, critical micelle concentration, and physical form. The micelle preparation method was optimized to achieve higher DEX solubility using exploratory model. Polymer–polymer interaction was found to be the prime cause of poor solubility of DEX in nanomicelles. Predictive model was generated to determine DEX and polymer amounts to achieve optimal formulation with 0.1% *w/v* DEX solubility. Modified film hydration method significantly enhanced the DEX entrapment in nanomicelles by overcoming the negative influence of polymer crystallization. Optimal nanomicelles were spherical in shape with unimodel size distribution. The data from *ex vivo* permeability and rigid nanomicelle core indicate that these nanomicelles may have the potential to deliver DEX and other hydrophobic anti-inflammatory agents such as rapamycin to the back of the eye following topical route for the treatment of intermediate to posterior segment uveitis. In further studies, we aim to prepare nanomicelles of various sizes using DOE. Furthermore, the effects of nanomicelle size on transport across the excised rabbit sclera will be determined for their potential to deliver drugs to the intermediate and posterior segments following topical administration. The nanomicelles of optimal size will also be tested in an *in vivo* rabbit model to confirm the efficacy of the optimal formulation.

ACKNOWLEDGMENTS

This research has been supported by grants R01 EY 09171-14 and R01 EY 10659-12 from the National Health Institute. The authors would like to thank Dr. James Murowchick from the School of Arts and Sciences, Department of Geosciences for XRD analysis and valuable discussion on the results and Dr. Deep Kwatra from The University of Kansas, Department of Molecular & Integrative Physiology for the help in formatting the images.

REFERENCES

1. Nussenblatt RB. The natural history of uveitis. Int Ophthalmol. 1990;14(5–6):303–8.
2. Gaudana R, Ananthula HK, Parenky A, Mitra AK. Ocular drug delivery. AAPS J. 2010;12(3):348–60.
3. Gaudana R, Jwala J, Boddu SH, Mitra AK. Recent perspectives in ocular drug delivery. Pharm Res. 2009;26(5):1197–216.
4. Taylor SR, Isa H, Joshi L, Lightman S. New developments in corticosteroid therapy for uveitis. Ophthalmologica. 2010;224 Suppl 1:46–53.
5. Lowder C, Belfort Jr R, Lightman S, Foster CS, Robinson MR, Schiffman RM, *et al*. Dexamethasone intravitreal implant for noninfectious intermediate or posterior uveitis. Arch Ophthalmol. 2011;129(5):545–53.
6. Robert H Janigian Jr, Jr RHJ. Uveitis evaluation and treatment 2012 [updated 08/20/201206/25/2013]. Available from: http://emedicine.medscape.com/article/1209123-overview.
7. Saraiya NV, Goldstein DA. Dexamethasone for ocular inflammation. Expert Opin Pharmacother. 2011;12(7):1127–31.
8. Couch SM, Bakri SJ. Intravitreal triamcinolone for intraocular inflammation and associated macular edema. Clin Ophthalmol. 2009;3:41–7.
9. Kim SH, Lutz RJ, Wang NS, Robinson MR. Transport barriers in transscleral drug delivery for retinal diseases. Ophthalmic Res. 2007;39(5):244–54.
10. HariKrishna A, Ravi V, Megha B, Mitra A. Bioavailability. Philadelphia: Lippincott Williams & Wilkins; 2009.
11. Tang DL, Song F, Chen C, Wang XL, Wang YZ. A pH-responsive chitosan-b-poly(p-dioxanone) nanocarrier: formation and efficient antitumor drug delivery. Nanotechnology. 2013;24(14):145101.
12. Gu Q, Xing JZ, Huang M, He C, Chen J. SN-38 loaded polymeric micelles to enhance cancer therapy. Nanotechnology. 2012; 23(20):205101.
13. Zhang Z, Mei L, Feng SS. Paclitaxel drug delivery systems. Expert Opin Drug Deliv. 2013;10(3):325–40.
14. Sun M, Su X, Ding B, He X, Liu X, Yu A, *et al*. Advances in nanotechnology-based delivery systems for curcumin. Nanomedicine. 2012;7(7):1085–100.
15. Amrite AC, Kompella UB. Size-dependent disposition of nanoparticles and microparticles following subconjunctival administration. J Pharm Pharmacol. 2005;57(12):1555–63.
16. Inokuchi Y, Hironaka K, Fujisawa T, Tozuka Y, Tsuruma K, Shimazawa M, *et al*. Physicochemical properties affecting retinal drug/coumarin-6 delivery from nanocarrier systems via eyedrop administration. Investig Ophthalmol Vis Sci. 2010;51(6):3162–70.
17. Park SH, Choi BG, Joo MK, Han DK, Sohn YS, Jeong B. Temperature-sensitive poly(caprolactone-co-trimethylene carbonate)−poly(ethylene glycol)−poly(caprolactone-co-trimethylene carbonate) as in situ gel-forming biomaterial. Macromolecules. 2008;41(17):6486–92.
18. Gou M, Men K, Shi H, Xiang M, Zhang J, Song J, *et al*. Curcumin-loaded biodegradable polymeric micelles for colon cancer therapy in vitro and in vivo. Nanoscale. 2011;3(4):1558–67.
19. Kalyanasundaram K, Thomas JK. Environmental effects on vibronic band intensities in pyrene monomer fluorescence and their application in studies of micellar systems. J Am Chem Soc. 1977;99(7):2039–44.
20. Basu Ray G, Chakraborty I, Moulik SP. Pyrene absorption can be a convenient method for probing critical micellar concentration (cmc) and indexing micellar polarity. J Colloid Interface Sci. 2006;294(1):248–54.
21. Gagarinova VM, Alferov VP, Kuznetsov VP, Ostrovskaia SA, Lapis GA, Piskareva NA. [Human leukocytic interferon as an agent for emergency prevention of influenza and other acute respiratory diseases in children's preschool institutions]. Pediatriia. 1990;101B(11):74-8. PubMed PMID: 2150098. Epub 1990/01/01. Chelovecheskii leikotsitarnyi interferon kak sredstvo ekstrennoi profilaktiki grippa i drugikh ORZ v detskikh doshkol'nykh kollektivakh. rus.
22. Lin HR, Chang PC. Novel pluronic-chitosan micelle as an ocular delivery system. J Biomed Mater Res B Appl Biomater. 2013;101(5):689–99.
23. Boddu SH, Jwala J, Vaishya R, Earla R, Karla PK, Pal D, *et al*. Novel nanoparticulate gel formulations of steroids for the treatment of macular edema. J Ocul pharmacol Ther Off J Assoc Ocul Pharmacol Ther. 2010;26(1):37–48.
24. Choi SH, Park TG. Hydrophobic ion pair formation between leuprolide and sodium oleate for sustained release from biodegradable polymeric microspheres. Int J Pharm. 2000;203(1–2):193–202.
25. Duvvuri S, Gaurav Janoria K, Mitra AK. Effect of polymer blending on the release of ganciclovir from PLGA microspheres. Pharm Res. 2006;23(1):215–23.
26. Earla R, Boddu SH, Cholkar K, Hariharan S, Jwala J, Mitra AK. Development and validation of a fast and sensitive bioanalytical method for the quantitative determination of glucocorticoids—quantitative measurement of dexamethasone in rabbit ocular matrices by liquid chromatography tandem mass spectrometry. J Pharm Biomed Anal. 2010;52(4):525–33.
27. Gaudana R, Parenky A, Vaishya R, Samanta SK, Mitra AK. Development and characterization of nanoparticulate

formulation of a water soluble prodrug of dexamethasone by HIP complexation. J Microencapsul. 2011;28(1):10–20.
28. ChemAxon. [cited 2013 7/8/13]. Available from: http://www.chemicalize.org/structure/#!mol=honokiol&source=calculate.
29. Gong C, Wei X, Wang X, Wang Y, Guo G, Mao Y, *et al*. Biodegradable self-assembled PEG-PCL-PEG micelles for hydrophobic honokiol delivery: I. Preparation and characterization. Nanotechnology. 2010;21(21):215103.
30. ChemAxon. [cited 2013 07/09/2013]. Available from: http://www.chemicalize.org/structure/#!mol=50-02-2&source=fp.
31. Palmer D, Levina M, Douroumis D, Maniruzzaman M, Morgan DJ, Farrell TP, *et al*. Mechanism of synergistic interactions and its influence on drug release from extended release matrices manufactured using binary mixtures of polyethylene oxide and sodium carboxymethylcellulose. Colloids surf B, Biointerfaces. 2013;104:174–80.
32. Hamalainen KM, Kananen K, Auriola S, Kontturi K, Urtti A. Characterization of paracellular and aqueous penetration routes in cornea, conjunctiva, and sclera. Investig Ophthalmol Vis Sci. 1997;38(3):627–34.